

6. S. Skupsky, R. W. Short, T. Kessler, R. S. Craxton, S. Letzring, and J. M. Soures, *J. Appl. Phys.* **66**, 3456 (1989).
7. S. E. Bodner, *J. Fusion Energy* **1**, 221 (1981).
8. D. K. Bradley, T. Boehly, D. L. Brown, J. Delettrez, W. Seka, and D. Smith, in *Laser Interaction and Related Plasma Phenomena*, edited by H. Hora and G. H. Miley (Plenum Press, New York, 1991), Vol. 9, pp. 323–334.
9. B. L. Henke and P. A. Jaanimagi, *Rev. Sci. Instrum.* **56**, 1537 (1985).
10. LLE Review **36**, 150 (1988).
11. M. C. Richardson, R. L. Keck, S. A. Letzring, R. L. McCrory, P. W. McKenty, D. M. Roback, J. M. Soures, C. P. Verdon, S. M. Lane, and S. G. Prussin, *Rev. Sci. Instrum.* **57**, 1737 (1986).
12. S. W. Haan, *Phys. Rev. A* **39**, 5812 (1989).
13. H. Takabe *et al.*, *Phys. Fluids* **28**, 3676 (1985).
14. R. L. McCrory, J. M. Soures, C. P. Verdon, S. Skupsky, T. J. Kessler, S. A. Letzring, W. Seka, R. S. Craxton, R. Short, P. A. Jaanimagi, M. Skeldon, D. K. Bradley, J. Delettrez, R. L. Keck, H. Kim, J. P. Knauer, R. L. Kremens, and F. J. Marshall, *Plasma Physics and Controlled Fusion* **31**, 1517 (1989).

1.B A Practical Nonlocal Model for Electron Heat Transport in Laser Plasmas

Computer simulations of electron heat transport, using the Fokker-Planck (FP) equation under conditions relevant to inertial-confinement fusion (ICF), have revealed inadequacies in the classical heat-flow model $\mathbf{q}_{SH} = -\kappa_{SH}\nabla T$ (where κ_{SH} is the Spitzer-Härm heat coefficient and T is the electron temperature in energy units).^{1,2} These inadequacies appear in the form of excessive heat flux under sharp temperature gradients, and in the lack of preheat due to long mean-free-path electrons ahead of the main heat front. Although the first inadequacy has been overcome to some extent with the use of flux limiters,³ there are cases, for example involving thermal smoothing,² when flux limiting is totally ineffective. As for the second inadequacy, in order to properly account for preheat phenomena, one has to resort to more sophisticated nonlocal heat-transport models, such as the FP equation or convolution formulas.

The use of convolution techniques has been suggested as a simpler, and computationally more efficient, alternative to solving the full FP equation for the electrons.^{4–13} The basic principle behind this approach is to convolve the

local heat flux q_{SH} with some appropriate kernel in configuration space so as to obtain (to some degree of approximation) the more accurate FP heat flow q_{FP} . The first practical convolution formula (also known as nonlocal heat-flow formula) was proposed by Luciani, Mora, and Virmont⁵

$$q_{LMV}(x) = \int_{-\infty}^{\infty} dx' \frac{q_{SH}(x')}{2a\lambda_e(x')} \exp[-\theta(x, x')] \quad 1(a)$$

where

$$\theta(x, x') = \left| \frac{1}{a\lambda_e(x')n(x')} \int_{x'}^x dx'' n(x'') \right| \quad 1(b)$$

is the number of stopping lengths between x and x' (sometimes referred to as optical depth) of an electron of temperature $T(x')$, $\lambda_e = T^2/4\pi n e^4 (Z+1)^{1/2} \ln \Lambda$ is its stopping length, and a is a free parameter. Here, the Coulomb logarithm (assumed the same for electrons and ions) is denoted by $\ln \Lambda$, n is the electron number density, e is the electronic charge, and Z is the ionic charge number. Despite the fact that this formula (referred to from now on as LMV) was not originally derived from first principles, it does have certain desirable properties: it gives flux inhibition under sharp temperature gradients, it can predict preheat ahead of the main heat front, and it yields the classical result in the collisional limit. Several subsequent papers by the same and other authors have attempted to justify and improve upon the LMV model.^{7,8} Using a different approach, Albritton, Williams, Bernstein, and Swartz derived a more complicated formula by directly solving a simplified form of the FP equation. Their model (to be referred as AWBS) has likewise been improved upon by others.^{9,10}

Despite the success of most nonlocal formulas in modeling heat transport under idealized laser-fusion conditions (i.e., with no hydrodynamics and high initial temperatures), to the best of our knowledge there have been no comparisons made with FP simulations under realistic ICF conditions, where a fuel pellet is imploded under laser irradiation. Moreover, Prasad and Kershaw¹¹ have recently suggested that there may be inherent numerical difficulties associated with the implementation of certain nonlocal models in hydrodynamic codes.

The aim of this article is to give a brief review of the nonlocal heat-flow models LMV and AWBS, discuss their limitations, propose an alternative model, and resolve the numerical problems in dealing with their implementation. Also, in order to adequately test the new nonlocal model, comparisons are made with the one-dimensional (1-D) version of the FP code SPARK,² which has been improved and changed to Lagrangian form.

Nonlocal Heat-Flow Formulas

The most general form of the convolution formula in 1-D is given by

$$q(x) = \beta^{-1} \int_{-\infty}^{\infty} dx' q_{SH}(x') G(x, x'), \quad (2)$$

where G is the delocalization kernel and $\beta = \int G dx'$ is a normalization factor.

A. The LMV and AWBS Models

Comparing Eq. (2) to Eq. (1) shows that for the LMV model

$$G_{\text{LMV}}(x, x') = \frac{\exp[-\theta(x, x')]}{2a\lambda_e(x')}, \quad (3)$$

where $a = 32$. This value of a was chosen by Luciani, Mora, and Virmont⁵ by comparison with FP code simulations.

The AWBS formula can be derived directly from the following simplified form of the FP equation,⁶

$$-\frac{\partial}{\partial x} \left[\frac{\lambda_{90}}{3} \frac{\partial (f_{\text{MB}} + \delta f)}{\partial x} \right] = \frac{m\nu^2}{\lambda_\epsilon} \frac{\partial \delta f}{\partial \epsilon}, \quad (4)$$

where f_{MB} is the Maxwell-Boltzmann (MB) distribution function, δf is a correction to f_{MB} , $\lambda_{90} = (m\nu^2)^2/4\pi n e^4 (Z \ln \Lambda_{ei} + \ln \Lambda_{ee})$ is the 90° electron angular-scattering mean-free path, $\lambda_\epsilon = (m\nu^2)^2/4\pi n e^4 \ln \Lambda_{ee}$ is the energy-loss mean-free path, and $\epsilon = m\nu^2/2 - e\phi$ is the total energy variable. The terms on the LHS and RHS of Eq. (4) represent contributions due to spatial diffusion and energy loss, respectively. By further assuming that $\epsilon \gg -e\phi$, Eq. (4) can be solved analytically to yield the following nonlocal heat-flow formula:⁶

$$\{j, q_{\text{AWBS}}\} = -\frac{(\lambda_{90}/\lambda_\epsilon)^{1/2}}{4\pi(3m)^{1/2}} \int_{-\infty}^{\infty} dx' n T^{-1/2} \{1, T\} \left[\frac{\partial T}{\partial x'} \{I, K\} - \frac{e\partial\phi_{\text{NL}}}{\partial x'} \{J, L\} \right]. \quad (5)$$

Here, j is the electric current (which is zero for 1-D thermal transport), and ϕ_{NL} is the nonlocal contribution to the electric potential. The propagators I , J , K , and L have been defined by Albritton *et al.*⁶ in terms of integral functions. Although the contribution of the electric field to the heat flow has been introduced in an explicit form, it is possible to recast Eq. (5) into the general form of Eq. (2).^{9,11,12} In fact, like the LMV formula, Eq. (5) reduces to the classical expression q_{SH} in the collisional limit.

The validity of both the LMV and the AWBS model relies on the following important assumptions: (1) The kernel G varies on the slow hydrodynamic time scale, rather than the fast time scale of the evolution of the electron-distribution function. This allows the incorporation of the nonlocal model in fluid codes, where the numerical integration time is governed mainly by the hydrodynamics of the plasma. (2) A small group of fast unthermalized electrons (with energies of about $7T$) are responsible for carrying the bulk of the heat flow, as compared to the thermalized MB distribution of background electrons. Such an assumption permits a simplification of the original FP equation, making it easier to solve analytically. (3) The plasma is of infinite extent. The main implication of this last assumption is that special care is needed in dealing with the spatial boundaries.

The reliability of nonlocal models is normally assessed by comparing their predictions to FP simulations. These comparisons have demonstrated varying degrees of success for the LMV model (and variations of it), and relatively more success for the AWBS model.^{5-10,12,13} Unfortunately, because of computational limitations in the FP simulations, the comparisons have usually been restricted to motionless fluids, high initial plasma temperatures (~100 eV), and short laser pulses (~100 ps).

A simpler, but potentially more useful, test consists of calculating the thermal decay of a temperature perturbation in a uniform plasma.¹⁴ The energy equation (neglecting hydrodynamics)

$$\frac{3}{2}n \frac{\partial T}{\partial t} + \nabla \cdot \mathbf{q} = 0, \tag{6}$$

is solved with the initial condition $T(x, t = 0) = T_0 + \delta T(0)\exp(ikx)$ to yield $\delta T(t) \propto \exp(-\gamma t)$. Assuming classical transport, the thermal decay rate is given by $\gamma_{SH} = 2k^2\kappa_{SH}/3n$. We can then apply the same perturbation to the FP equation, numerically calculate the asymptotic decay rate defined by $\gamma_{FP} = 2k^2\kappa_{FP}/3n$, and obtain κ_{FP}/κ_{SH} for a given wave number k . This test has been done using the FP code SPARK, the results of which are plotted in Fig. 48.8 (solid circles) as a function of $k\lambda_e$. As expected, in the long-wavelength limit ($k\lambda_e \rightarrow 0$) $\kappa_{FP}/\kappa_{SH} \rightarrow 1$. As the perturbation wavelength becomes much shorter than λ_e , a significant reduction in the effective κ is observed. This effect is not new and has been previously discussed in the context of ion waves,⁴ thermal smoothing,² and laser thermal filamentation.¹⁵ The flux inhibition occurs as a result of nonlocal transport of heat-carrying electrons (with energies of about $7T$) across several wavelengths.

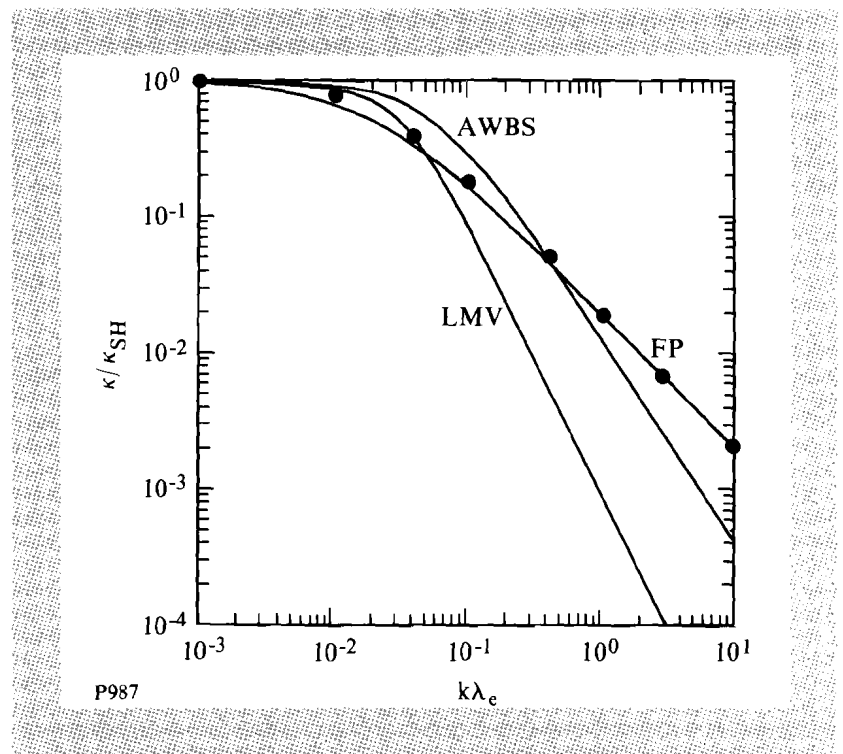


Fig. 48.8 Heat-conductivity spectrum. Ratio of effective conductivity κ to Spitzer-Härm conductivity κ_{SH} as a function of $k\lambda_e$, where k is the perturbation wave number and λ_e is the electron delocalization length. Filled circles correspond to SPARK simulations.

It is straightforward to apply the thermal decay test to the nonlocal heat-flow models discussed in this article. Substituting the LMV formula into Eq. (6) and taking the Fourier transform we obtain¹⁴

$$\frac{\kappa_{\text{LMV}}}{\kappa_{\text{SH}}} = \frac{1}{1 + (ak\lambda_e)^2}. \quad (7)$$

The ratio $\kappa_{\text{LMV}}/\kappa_{\text{SH}}$ is plotted in Fig. 48.8 as a function of $k\lambda_e$. Repeating the same procedure with the AWBS formula requires numerical integration of the propagators.¹⁶ The result is also plotted in Fig. 48.8.

By comparing the curves in Fig. 48.8, it is clear that neither the LMV nor the AWBS models agree with the FP results, with the former giving the worse agreement. The discrepancy between SPARK simulation results and the AWBS model could be caused by two approximations in the latter: the assumption that $\partial f/\partial t = 0$, and the neglect of energy upscattering for the heat-carrying electrons. For large $k\lambda_e$ both $\kappa_{\text{LMV}}/\kappa_{\text{SH}}$ and $\kappa_{\text{AWBS}}/\kappa_{\text{SH}}$ scale as $1/(k\lambda_e)^2$, whereas $\kappa_{\text{FP}}/\kappa_{\text{SH}}$ has a $1/k\lambda_e$ scaling.¹⁷ Prasad and Kershaw¹¹ have recently demonstrated that the $1/(k\lambda_e)^2$ asymptotic dependence of the LMV and AWBS models can lead to unphysical results. They show that, since the decay rate becomes independent of k for large $k\lambda_e$ (i.e., γ_{LMV} and $\gamma_{\text{AWBS}} \propto 2\kappa_{\text{SH}}/3n\lambda_e^2$ as $k\lambda_e \rightarrow \infty$), sharp features in temperature will persist indefinitely.

Before proceeding further, it is important to realize that the thermal decay calculation, previously described, is not the only useful test for a nonlocal heat-flow model. It has been shown, for example, that ion motion can play an important role in the energy-transport process. Indeed, ion motion may lead to a phase mismatch between ∇T and \mathbf{q} .⁴ Also, inverse-bremsstrahlung (IB) heating can significantly modify the electron-distribution function and hence lead to a modified $\kappa_{\text{FP}}/\kappa_{\text{SH}}$.⁸ This phenomenon has recently been investigated in the context of laser filamentation, where it was shown that $[\kappa_{\text{FP}}/\kappa_{\text{SH}}]_{\text{IB}} \approx 1/[1 + (30k\lambda_e)^{4/3}]$.¹⁵ One may, therefore, conclude that since the *correct* kernel is problem dependent, caution is necessary when applying nonlocal transport models to situations previously untested by the more accurate FP simulations.

B. An Alternative Nonlocal Heat-Transport Model

The basis of our new model lies in the assumption that the thermal decay spectrum calculated by the FP code SPARK and plotted in Fig. 48.8, provides the most essential information for nonlocal transport. In order to arrive at a useful formula, the spectrum is initially fitted to the FP results, i.e., $\kappa_{\text{FP}}/\kappa_{\text{SH}} \approx 1/(1 + ak\lambda_e)$, by choosing $a = 50$ (see FP curve in Fig. 48.8). It is now straightforward to take the inverse Fourier transform of this equation and obtain the following kernel in configuration space:

$$G(x, x') = \frac{1}{\pi a \lambda(x')} [-\sin(\theta)\text{si}(\theta) - \cos(\theta)\text{Ci}(\theta)], \quad (8)$$

where si and Ci are the sine and cosine integrals, respectively.¹⁸ In order to improve the accuracy of the model, the value of θ [given by Eq. (1b)] has been modified by redefining the electron stopping length as $\lambda_e^* = T^2/4\pi n e^4 (Z^* \phi \ln \Lambda_{ei} \ln \Lambda_{ee})^{1/2}$, where $Z^* = \langle Z^2 \rangle \ln \Lambda_{ei} / \langle Z \rangle \ln \Lambda_{ee}$ is the effective charge number ($\langle \rangle$ denotes an average over the ion species) and $\phi = (Z^* + 4.2) / (Z^* + 0.24)$. The inclusion of the factor ϕ is an attempt to correct for the high- Z approximation in the original nonlocal models.

It is of interest to note that for short wavelengths (large $k\lambda_e$) the FP results for κ/κ_{SH} (see Fig. 48.8) lie between the (local) SH value $\kappa/\kappa_{SH} = 1$ and the LMV results, implying that the LMV kernel (3) is “too delocalized.” Therefore, it is not surprising that $G(x, x')$ lies, in a sense, “between” the SH kernel $G_{SH}(x, x') = \delta(x - x')$ and $G_{LMV}(x, x')$, having some of the properties of each. Both $G(x, x')$ and $G_{SH}(x, x')$ diverge for $x = x'$, whereas $G_{LMV}(x, x')$ does not:

$$\lim_{x' \rightarrow x} G(x, x') = \infty, \quad \lim_{x' \rightarrow x} G_{SH}(x, x') = \infty,$$

but

$$\lim_{x' \rightarrow x} G_{LMV}(x, x') = \frac{1}{2a\lambda_e(x)}. \quad (9)$$

On the other hand, the contribution to the heat-flow integral from an infinitesimal region near $x = x'$ vanishes for $G(x, x')$ and $G_{LMV}(x, x')$, but not for $G_{SH}(x, x')$:

$$\lim_{\delta \rightarrow 0} \int_{-\delta}^{\delta} G(x, x') dx' = 0, \quad \lim_{\delta \rightarrow 0} \int_{-\delta}^{\delta} G_{LMV}(x, x') dx' = 0,$$

but

$$\lim_{\delta \rightarrow 0} \int_{-\delta}^{\delta} G_{SH}(x, x') dx' = 1. \quad (10)$$

Thus, $G(x, x')$ is more sharply peaked at $x = x'$ than $G_{LMV}(x, x')$ but less sharply than at $G_{SH}(x, x')$, so that it provides an intermediate level of delocalization.

Numerical Implementation

There are two potential problems with the numerical implementation of nonlocal heat-transport formulas: (a) The inability to smooth out sharp features in temperature profiles, and (b) the possible occurrence of negative values of κ/κ_{SH} , which can lead to anti-diffusion instabilities (with the eventual generation of negative temperature distributions). The first problem, discussed in detail in the previous section, results from the $1/(k\lambda_e)^2$ dependence of the LMS and AWBS models in the limit as $k\lambda_e \rightarrow \infty$. One solution is to use a nonlocal model based on FP simulation, which yields a $1/k\lambda_e$ asymptotic dependence, as described in Part (B) of this article. The second problem is not inherent to the convolution model itself but is a general feature of electron heat transport. FP simulations, under conditions relevant

to ICF, have shown that it is possible for the effective heat flow to be in the direction of ∇T (i.e., up the temperature gradient).^{1,2}

The occurrence of a negative conductivity, defined by $\kappa_{FP} = -\mathbf{q}_{FP}/\nabla T < 0$, need not be a problem provided it is restricted to regions of the plasma where the heat flow is relatively unimportant. Fortunately, extensive FP simulations using SPARK have indicated that this is indeed the case. The effective conductivity tends to become negative mainly in the corona, where the plasma is fairly isothermal, and the magnitude of the heat flow is generally much smaller than in the overdense region. We therefore propose that a simple solution to the problem is to enforce $\kappa/\kappa_{SH} = 1$, whenever κ/κ_{SH} is initially negative. Thus the anti-diffusion instability is avoided by requiring a positive conductivity. However, when the conductivity is initially positive, the scheme still allows for the possibility of flux inhibition ($\kappa/\kappa_{SH} < 1$) and enhanced heat flux ($\kappa/\kappa_{SH} > 1$).

In practice, the implementation of the numerical scheme involves time-implicit differencing of Eq. (6) in conservative form, i.e.,

$$\begin{aligned} \frac{3}{2}n(T_k^{n+1} - T_k^n) &= \frac{\Delta t}{\Delta x_k}(-q_{k+1/2} + q_{k-1/2})^{n+1} \\ &= \frac{\Delta t}{\Delta x_k} \left[\frac{\kappa_{k+1/2}^n}{\Delta x_{k+1/2}} (T_{k+1} - T_k)^{n+1} - \frac{\kappa_{k-1/2}^n}{\Delta x_{k-1/2}} (T_k - T_{k-1})^{n+1} \right], \end{aligned} \quad (11)$$

where the effective κ is defined by

$$\kappa_{k+1/2} = -\frac{\Delta x_{k+1/2}}{(T_{k+1} - T_k)\beta_{k+1/2}} \int_{x_{k+1/2}-d}^{x_{k+1/2}+d} dx' G(x_{k+1/2}, x') q_{SH}(x'). \quad (12)$$

Here we have assumed planar geometry, with x_k and $x_{k+1/2}$ denoting cell centers and boundaries, respectively. The normalization factor is given by

$$\beta_{k+1/2} = \int_{x_{k+1/2}-d}^{x_{k+1/2}+d} dx' G(x_{k+1/2}, x'). \quad (13)$$

Since the plasma is not of infinite extent, the range of integration is taken from $x_{k+1/2} - d$ to $x_{k+1/2} + d$, where d is large enough to provide several stopping lengths between $x_{k+1/2}$ and $x_{k+1/2} \pm d$, i.e., $\theta(x_{k+1/2}, x_{k+1/2} \pm d) \gg 1$. By adopting multiple plasma images, the effective κ defined by Eq. (12) also ensures zero heat flux at the plasma boundaries, as is normally required for plasma simulations.

We note from Eq. (12) that κ is not defined when $T_k = T_{k+1}$ (as would be the case in regions of the simulation yet unperturbed by the heat front). We avoid this problem by evaluating $q_{k+1/2}$ at the n th time level (i.e., explicitly) whenever $|T_{k+1} - T_k| < \eta |T_{k+1} + T_k|$, where η is a small number (say 10^{-6}).¹³ Another alternative would have been to solve Eq. (11) with κ defined at the

($n+1$)th time level. Such an approach, which is the one adopted by Prasad and Kershaw,¹¹ requires a full-matrix inversion at each time step, involving more computer time than the present method. Our approach also has the added advantage of being more easily appended to an ordinary hydrodynamic code, since it simply redefines κ .¹⁹ In the limit as $\Delta t \rightarrow 0$ both methods are equivalent.

To test the viability of the nonlocal model we have used SPARK to simulate the heat transport in an idealized plasma, with fixed ions and an initial temperature of 25 eV, irradiated by 351-nm laser at a constant intensity of 5×10^{14} W/cm² over 100 ps. Figure 48.9(a) shows the temperature and density (normalized to the critical density n_c) profiles at the end of the simulation. The solid, dashed, and dash-dotted curves refer to the FP, SH, and nonlocal transport calculations, respectively. The corresponding magnitudes of the heat flow are plotted in Fig. 48.9(b).

A comparison of the FP and SH curves in Fig. 48.9 serves to illustrate the typical features of nonlocal transport: flux inhibition of the main heat front, preheat in the cold overdense plasma, and heat flux directed up the temperature gradient in the corona. The simulation using the new nonlocal heat-transport formula is shown to be in reasonable agreement with the FP results. Despite the potential destabilizing influence of the anti-diffusion instability, we were also able to perform the nonlocal formula calculation allowing for $\kappa/\kappa_{SH} < 0$. The main effect of forcing $\kappa/\kappa_{SH} > 0$ is to flatten the

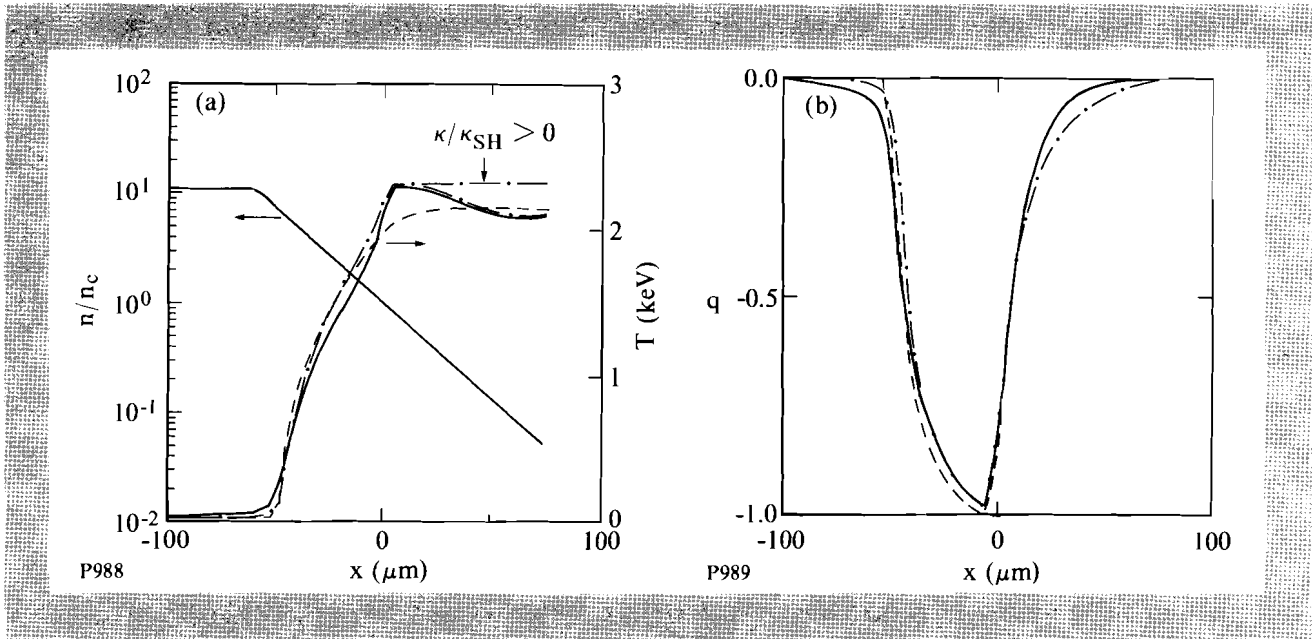


Fig. 48.9
 Idealized plasma simulation. Plots of (a) electron number density (normalized to the critical density) and temperature in keV, and (b) heat flow (in arbitrary units) as functions of space. Solid, dashed, and dash-dotted curves correspond to FP, SH, and nonlocal heat-flow formula simulations, respectively.

coronal temperature profile (see curve $\kappa/\kappa_{\text{SH}} > 0$ in Fig. 48.9). However, the influence on the overdense temperature distribution is negligible.

Simulation of a Laser-Driven Implosion

Until now, the accuracy of nonlocal models has been tested under idealized plasma conditions, such as those described in the previous section. It is, therefore, important to test them under more realistic conditions pertaining to laser-driven ICF. These normally involve variations of several orders of magnitude in temperature and density, hydrodynamic effects, and spherical convergence. In order to simulate these conditions the 1-D version of the FP code SPARK has been improved and converted to spherical geometry in a Lagrangian scheme.

Here, we model the implosion of a fully ionized 10- μm -CH shell of 150- μm radius, irradiated by a 351-nm laser with a 600-ps-FWHM Gaussian pulse of peak intensity $5 \times 10^{14} \text{ W/cm}^2$. The target is initially at a temperature of 1 eV and is divided into 40 uniformly distributed 0.25- μm spatial cells. A nonuniform velocity mesh is used for the electron-distribution function, such that v_j is the velocity of the j th cell center (where $j = 1, \dots, 50$), $\Delta v_{j+1}/\Delta v_j = 1.08$ is the ratio of the widths of two adjacent velocity cells, and $(1/2)mv_{50}^2 = 18.6 \text{ keV}$ is the maximum energy group.

Figure 48.10 shows plots of electron number density (normalized to the critical density n_c) and temperature in electron volts. Early in the simulation (at -500 ps with respect to the peak of the laser pulse) the plasma is still relatively cold and collisional, so that there is little difference between SH (dashed curves) and FP (solid curves) results. The times 200 ps and 400 ps correspond to before and after the shock reaches the center of the target, respectively. Note that there is a significant difference between SH and FP calculations, both in terms of peak density, and ablation-surface temperature. As a result of $\sim 2 \text{ keV}$ coronal temperatures, electrons from that region are able to stream relatively unimpeded through the overdense plasma to deposit their energy at the ablation surface. This preheating phenomenon has the effect of degrading the compression efficiency, with a subsequent lowering of the target's peak density. This type of effect has also been reported by Mima *et al.* for CH targets illuminated by 531-nm laser light.²⁰

Although preheat is seen to cause a significant difference in the peak density, other observables, such as the total fractional absorption of light and implosion time, which are more sensitive to the penetration of the main heat front, remain relatively unaffected by the FP treatment. For these, closer agreement between FP and SH calculations can be obtained with the use of a simple flux limiter on the latter.

The previous simulation has been repeated with the use of the nonlocal model developed in this article. Results are plotted in Fig. 48.9 as dash-dotted curves. Comparison with the FP results shows the nonlocal model to be in reasonable agreement with the former, apart from a slight underestimation of preheat.

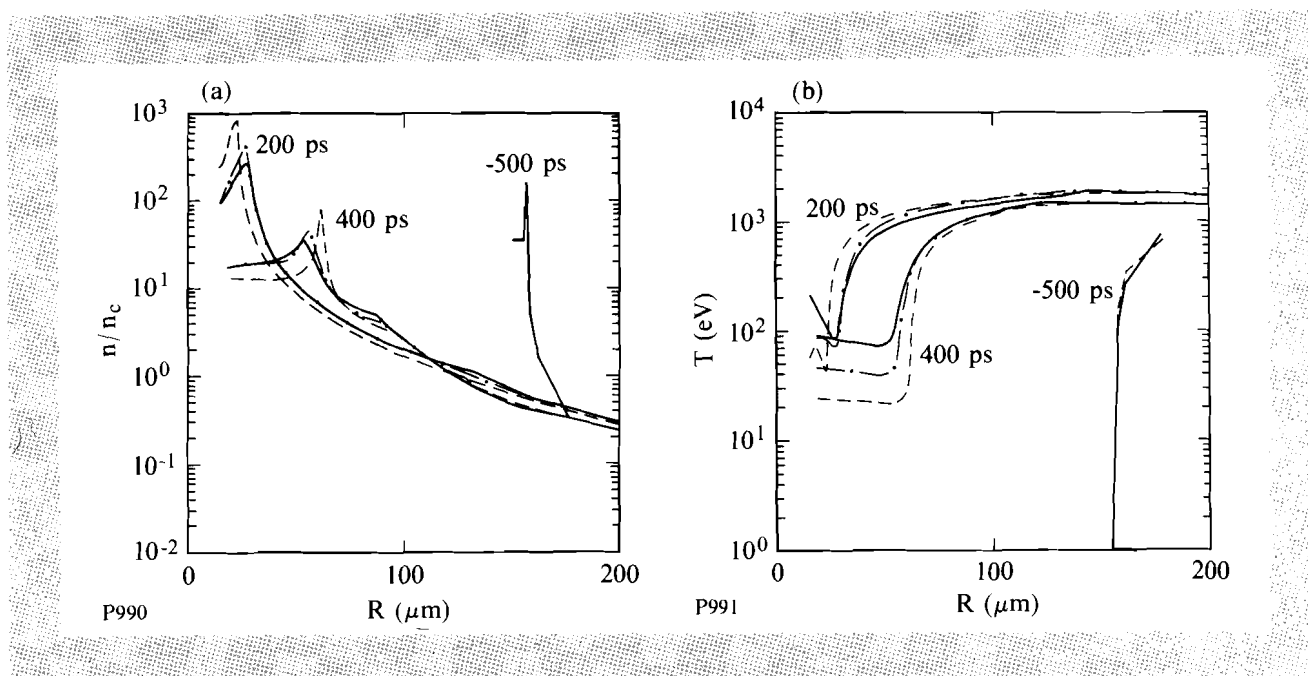


Fig. 48.10

Simulation of a laser-driven implosion. Plots of (a) electron number density and (b) temperature, as functions of space. Curves are identified as in Fig. 48.9.

It is important to point out at this stage that the accuracy of our nonlocal transport model is only as good as the accuracy of the FP model itself. Although the hydrodynamic and electron transport treatment in SPARK has been improved, the code still assumes full ionization (even at the initial temperature of 1 eV), an ideal equation of state, and no radiation effects. In particular, the inclusion of energy loss because of collisional ionization in the cold target could severely reduce the preheat caused by the long mean-free-path electrons. Radiation preheat is relatively weak in CH, but for higher- Z targets this type of preheat may dominate.

Summary and Conclusions

With the help of a simple test involving the decay of linear thermal waves, we have been able to assess the accuracy of two types of nonlocal formulas (initially developed by Luciani *et al.*⁵ and Albritton *et al.*⁶) by comparing their predictions with those based on FP simulations. The resulting spectrum of $\kappa/\kappa_{\text{SH}}$ as a function of $k\lambda_e$ indicates a potential problem that may arise in the numerical implementation of certain nonlocal models. The problem is associated with the functional behavior of $\kappa/\kappa_{\text{SH}}$ for large $k\lambda_e$. If $\kappa/\kappa_{\text{SH}} \propto 1/(k\lambda_e)^2$, as is the case for the LMV and AWBS models, the thermal decay rate becomes independent of k and sharp features in temperature profiles do not decay in any finite time. The spectrum of $\kappa_{\text{FP}}/\kappa_{\text{SH}}$ as a function of $k\lambda_e$ has also provided the basis for the derivation of a new nonlocal model that avoids this thermal decay problem.

Another difficulty associated with the practical implementation of nonlocal models has been their prediction of heat flux directed along ∇T , with the subsequent occurrence of anti-diffusion instabilities. A straightforward solution to this problem is to enforce SH heat flow whenever the situation $\mathbf{q} \cdot \nabla T > 0$ arises. The justification for this procedure comes from comparisons with full FP simulations under idealized plasma conditions. The model also compares reasonably well with a SPARK FP simulation of a laser-driven implosion of a fully ionized CH shell.

Our motivation for nonlocal heat-transport modeling of ICF targets has come from the prediction of significant preheat (resulting from coronal electrons) in the ablation region with a subsequent reduction in compression efficiency. However, it must be stressed that both the FP code and the convolution formula developed in this article have omitted ionization and radiation physics. The future inclusion of these phenomena could substantially mitigate the preheating effects presently discussed.

ACKNOWLEDGMENT

We would like to acknowledge many helpful discussions with J. R. Albritton, W. E. Alley, M. K. Prasad, R. A. Sacks, S. V. Weber, and E. A. Williams. While this manuscript was in progress we were made aware of similar work by M. K. Prasad and D. S. Kershaw. This work was supported by the U.S. Department of Energy Office of Inertial Confinement Fusion under agreement No. DE-FC03-85DP40200 and by the Laser Fusion Feasibility Project at the Laboratory for Laser Energetics, which is sponsored by the New York State Energy Research and Development Authority and the University of Rochester.

REFERENCES

1. A. R. Bell, R. G. Evans, and D. J. Nicholas, *Phys. Rev. Lett.* **46**, 243 (1981); J. R. Albritton, *Phys. Rev. Lett.* **50**, 2078 (1983); J. P. Matte, T. W. Johnston, J. Delettrez, and R. L. McCrory, *Phys. Rev. Lett.* **53**, 1461 (1984); A. R. Bell, *Phys. Fluids* **28**, 2007 (1985); T. H. Kho and M. G. Haines, *Phys. Fluids* **29**, 2665 (1986).
2. E. M. Epperlein, G. J. Rickard, and A. R. Bell, *Phys. Rev. Lett.* **61**, 2453 (1988); E. M. Epperlein, G. J. Rickard, and A. R. Bell, *Comput. Phys. Commun.* **52**, 7 (1988).
3. R. C. Malone, R. L. McCrory, and R. L. Morse, *Phys. Rev. Lett.* **34**, 721 (1975).
4. A. R. Bell, *Phys. Fluids* **26**, 279 (1983).
5. J. F. Luciani, P. Mora, and J. Virmont, *Phys. Rev. Lett.* **51**, 1664 (1983).
6. J. R. Albritton *et al.*, *Phys. Rev. Lett.* **57**, 1887 (1986).
7. J. F. Luciani, P. Mora, and R. Pellat, *Phys. Fluids* **28**, 835 (1985); J. F. Luciani, P. Mora, and A. Bendib, *Phys. Rev. Lett.* **55**, 2421 (1985); E. L. Lindman and K. Swartz, *Phys. Fluids* **29**, 2657 (1986); A. Bendib, J. F. Luciani, and J. P. Matte, *Phys. Fluids* **31**, 711 (1988).
8. J. F. Luciani and P. Mora, *Phys. Lett. A* **116**, 237 (1986).
9. F. Minotti and C. Ferro Fontán, *Phys. Fluids B* **2**, 1725 (1990).

10. J. R. Sanmartin, J. Ramirez, and R. Fernandez Feria, *Phys. Fluids B* **2**, 2519 (1990); G. Murtaza, A. Mirza, and M. S. Qaisar, *Phys. Lett. A* **144**, 164 (1990); G. Murtaza, A. Mirza, and M. S. Qaisar, *Plasma Phys. Control. Fusion* **33**, 215 (1991).
11. M. K. Prasad and D. S. Kershaw, *Phys. Fluids B* **1**, 2430 (1989).
12. P. A. Holstein and A. Decoster, *J. Appl. Phys.* **62**, 3592 (1987).
13. P. A. Holstein, J. Delettrez, S. Skupsky, and J. P. Matte, *J. Appl. Phys.* **60**, 2296 (1986).
14. E. M. Epperlein, "Electron Kinetics in Laser-Driven Inertial Confinement Fusion," to be published in *Proceedings of the Topical Conference on Research Trends in Nonlinear and Relativistic Effects in Plasmas*, San Diego, CA, February 1990; LLE Review **42**, 57 (1990).
15. E. M. Epperlein, *Phys. Rev. Lett.* **65**, 2145 (1990).
16. Numerical integration has been kindly provided by E. A. Williams (private communication).
17. J. R. Albritton and E. A. Williams (private communication).
18. W. Gautschi and W. F. Cahill, *Handbook of Mathematical Functions*, edited by M. Abramowitz and I. A. Stegun (Dover Publications, Inc., New York, 1970), p. 231.
19. This current version of the nonlocal heat-flow formula has been successfully added to the *LILAC* hydrodynamic code at the LLE, University of Rochester.
20. K. Mima *et al.*, *Laser Part. Beams* **7**, 487 (1989).